

AdaDM: Enabling Normalization for Image Super-Resolution

Jie Liu Jie Tang* Gangshan Wu

State Key Laboratory for Novel Software Technology, Nanjing University, China

jieliu@smail.nju.edu.cn, {tangjie, gswu}@nju.edu.cn

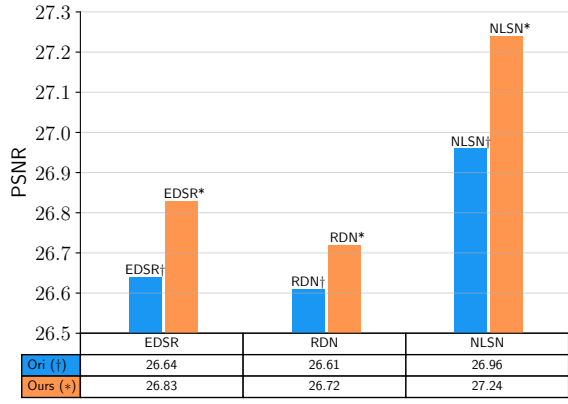
<https://github.com/njulj/AdaDM>

Abstract

Normalization like Batch Normalization (BN) is a milestone technique to normalize the distributions of intermediate layers in deep learning, enabling faster training and better generalization accuracy. However, in fidelity image Super-Resolution (SR), it is believed that normalization layers get rid of range flexibility by normalizing the features and they are simply removed from modern SR networks. In this paper, we study this phenomenon quantitatively and qualitatively. We found that the standard deviation of the residual feature shrinks a lot after normalization layers, which causes the performance degradation in SR networks. Standard deviation reflects the amount of variation of pixel values. When the variation becomes smaller, the edges will become less discriminative for the network to resolve. To address this problem, we propose an Adaptive Deviation Modulator (AdaDM), in which a modulation factor is adaptively predicted to amplify the pixel deviation. For better generalization performance, we apply BN in state-of-the-art SR networks with the proposed AdaDM. Meanwhile, the deviation amplification strategy in AdaDM makes the edge information in the feature more distinguishable. As a consequence, SR networks with BN and our AdaDM can get substantial performance improvements on benchmark datasets. Extensive experiments have been conducted to show the effectiveness of our method.

1. Introduction

Image Super-Resolution (SR) serves as a fundamental tool in image processing and computer vision. The goal of classical image SR is to reconstruct a high-fidelity High-Resolution (HR) image from a degraded Low-Resolution (LR) image. Since the pioneering work of SRCNN [6], Convolutional Neural Networks (CNN) have become the primary workhorse for image SR [7, 24, 14, 1, 21, 8, 42].



(a) PSNR Improvements.

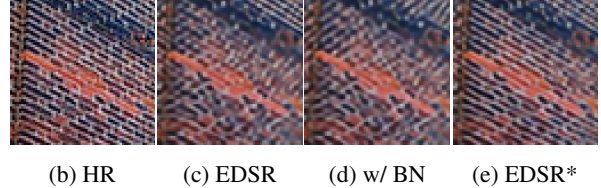


Figure 1: (a) PSNR improvements of EDSR [24], RDN [49] and NLSN [33] with BN+AdaDM on Urban100 $\times 4$ dataset. (b) HR patch from img098 in Urban100 dataset. (c) SR results of EDSR. (d) SR results of EDSR with BN layers. (e) SR results of EDSR with BN+AdaDM.

Early CNN-based SR networks, for example SRResNet [20], applied the ResNet [10] architecture to the super-resolution task. However, Lim *et al.* [24] found that the Batch Normalization (BN) layers in residual blocks damage the performance of SR networks. They speculate that BN layers get rid of range flexibility from networks by normalizing the features. As a result, they removed BN layers from the residual blocks and achieved substantial performance improvements. Inspired by this, most of the state-of-

*Corresponding author.

the-art SR networks exclude normalization layers in their building blocks. On the other hand, many SR networks are getting larger and larger in pursuit of extreme fidelity. When the network becomes deeper and wider, it will be very difficult to optimize without normalization layers. Since normalization layers have been successfully applied to various computer vision tasks for faster training and better generalization, we wonder whether they can be applied in SR networks without compromising performance.

In this paper, we show that normalization will reduce the standard deviation of feature pixels (*i.e.*, pixel deviation), which causes the performance degradation. Standard deviation reflects the amount of variation of pixel values. As the pixel deviation shrinks, the edge information in the feature becomes less discriminative. Figure 1d shows one sample output of the EDSR model with BN layers. As we can see, it looks more blurry and messy compared to the patch produced by original EDSR in Figure 1c, which indicates that the BN layers increase the difficulty of the network to resolve the edges. To address this problem, we propose an Adaptive Deviation Modulator (AdaDM) to amplify the pixel deviation of the features in cooperation with normalization layers. Figure 1e shows the SR patch produced by the EDSR model with BN layers and our AdaDM. It reconstructs the edges sharper and clearer than EDSR and EDSR with BN, which demonstrates the effectiveness of our AdaDM.

With the proposed AdaDM, we can successfully apply normalization layers in state-of-the-art SR networks without compromising performance. We insert BN layers and our AdaDM into the residual blocks of EDSR [24], RDN [49] and NLSN [33] to build three new models: EDSR*, RDN* and NLSN*. As shown in Figure 1a, the performance of the three models has been significantly improved since they can benefit from feature normalization, which shows the necessity of normalization in large models. Overall, the main contribution of this paper is to propose a novel AdaDM that can enable feature normalization in SR networks, which greatly improves the performance for high-fidelity SR. Code and pretrained models are available at <https://github.com/njulj/AdaDM>.

2. Related Work

2.1. Image Super-Resolution

In the past few years, numerous SR methods based on deep learning have been proposed [7, 19, 36, 38, 20, 9, 47, 22, 28, 11, 34, 26, 43, 37]. The pioneering work was done by [6], who first proposed a three-layer convolutional network (SRCNN) to learn an end-to-end mapping from LR to HR directly. Later, VDSR [16] and DRCN [17] increase the network depth to 20 and achieve notable improvements over SRCNN. EDSR [24] further increases the

network depth to about 165 layers by removing BN layers from the residual blocks [10]. [49] proposed to use dense connections [12] in a residual block to get a better performance. RCAN [48] uses the residual in residual (RIR) connections to train a very deep network that achieves excellent performance. Recently, many attention based SR networks [25, 25, 5, 27, 35, 33, 50, 30, 4, 23] are proposed to exploit the extreme fidelity of image SR. However, most of them do not use normalization layers because of the poor performance. Normalization like BN is a milestone technique in deep learning. It is a waste by simply abandoning BN in residual blocks. In this paper, we show that the proposed AdaDM can successfully enable BN layers in SR networks, which greatly improves the performance.

2.2. Feature Normalization

Following [45], we give a general formulation of feature normalization in the case of 2D images. A series of feature normalization techniques, including Batch Normalization (BN) [15], Layer Normalization (LN) [2], Instance Normalization (IN) [40] and Group Normalization (GN) [45], normalize the features as follows:

$$\hat{x}_i = \frac{x_i - \mu_i}{\sigma_i}, \quad (1)$$

where x is the intermediate feature of a network, and $i = (i_N, i_C, i_H, i_W)$ is a 4D vector indexing the features in (N, C, H, W) order. Here N , C , H and W denote the batch, channel, height and width dimensions, respectively.

In (1), μ and σ are the mean and standard deviation computed as:

$$\mu_i = \frac{1}{m} \sum_{k \in S_i} x_k, \quad \sigma_i = \sqrt{\frac{1}{m} \sum_{k \in S_i} (x_k - \mu_i)^2 + \epsilon}, \quad (2)$$

with ϵ as a small constant for numerical stability. The mean and standard deviation are computed within a set of pixels S_i , and m is the size of S_i . For BN, S_i is defined by:

$$S_i = \{k \mid k_C = i_C\}. \quad (3)$$

Here $k = (k_N, k_C, k_H, k_W)$, and k_C is the sub-index of k along the C axis. This means that pixels in the same channel are normalized together, *i.e.*, μ and σ are computed along the (N, H, W) axes. For LN, the set is:

$$S_i = \{k \mid k_N = i_N\}, \quad (4)$$

indicating that μ and σ are computed along the (C, H, W) axes for each sample. The details for IN and GN can be found in [45].

3. Motivation

For a better understanding, we first construct three toy residual blocks, *i.e.*, T1, T2 and T3, to illustrate the motivation behind our method. As shown in Figure 2, T1 contains

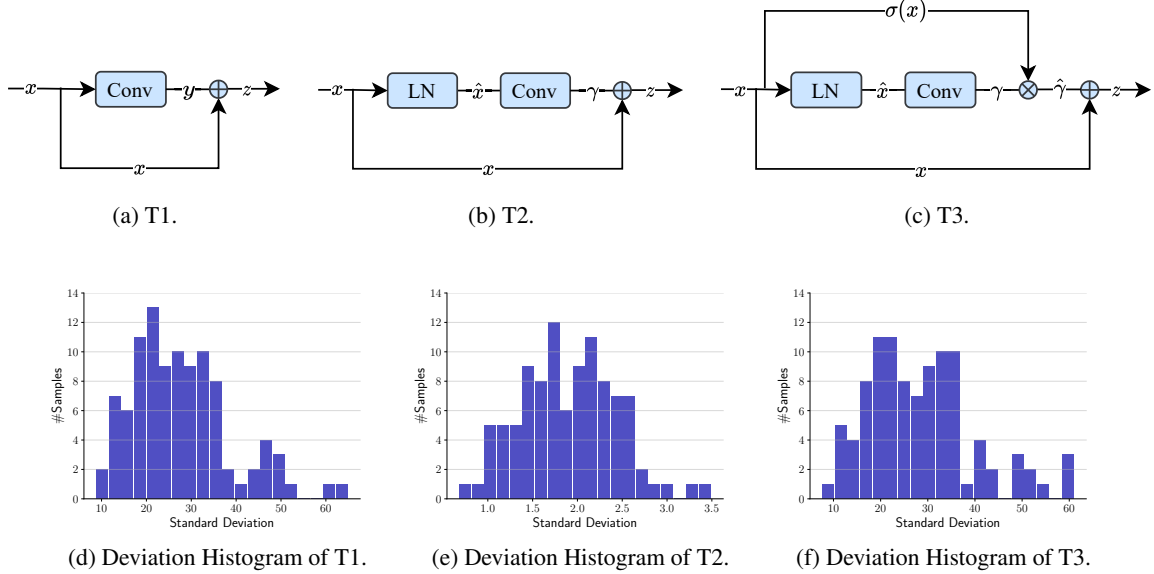


Figure 2: (a)-(c): Three toy residual blocks. (d)-(f): Deviation histograms of y , γ and $\hat{\gamma}$, respectively. The standard deviation is computed on the 100 images from Urban100 \times 2 dataset.

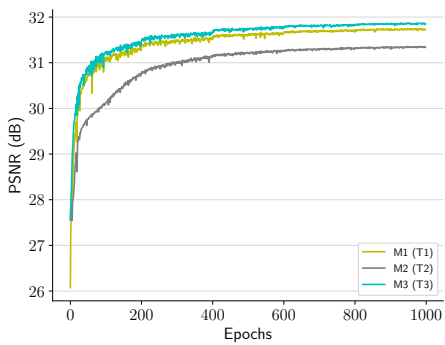


Figure 3: The learning curves of three toy SR models. Model M1/M2/M3 is constructed by using T1/T2/T3 as the building block. All the models are evaluated on Urban100 \times 2 dataset.

only one convolutional layer (Conv) in the residual branch. T2 is constructed by inserting a LN layer before the Conv layer. We use LN because it is easier to perform formal analysis than BN. T3 has the same layers as T2 except for the new element-wise multiplication layer. Next we will give a formal description of T2 and then discuss the effects of feature normalization from the perspective of pixel deviation. For simplicity, we remove the bias terms in Conv layers and turn off the affine transformation in LN layers.

It is worth noting that the following analysis is based on a forward propagation and we assume T1, T2 and T3 have the

same predefined weights. In Figure 2b, x is a single input sample with three axes (C, H, W), and \hat{x} is the transformed feature with LN. For LN, the mean and standard deviation are computed along the (C, H, W) axes, so we can compute \hat{x} as:

$$\hat{x} = \frac{x - \mu}{\sigma}, \quad (5)$$

where μ and σ are scalars shared by all pixels in x . Denote the function of the Conv layer as f_{Conv} , then the output γ can be computed by:

$$\gamma = f_{Conv}(\hat{x}) = f_{Conv}\left(\frac{x - \mu}{\sigma}\right). \quad (6)$$

According to the associativity of convolution to scalar multiplication, we can rewrite (6) as:

$$\gamma = \frac{1}{\sigma} f_{Conv}(x - \mu). \quad (7)$$

This formula can be further expanded using the distributivity:

$$\gamma = \frac{1}{\sigma} f_{Conv}(x) - \frac{1}{\sigma} f_{Conv}(\mu I). \quad (8)$$

Here I is the all-ones matrix with the same dimensions as x . In Figure 2a, the output of Conv layer can be written as:

$$y = f_{Conv}(x). \quad (9)$$

Comparing (8) and (9), we can find that the pixel distributions (e.g. mean and variation) of y has been reshaped by LN. In image SR, we are more concerned about the pixel

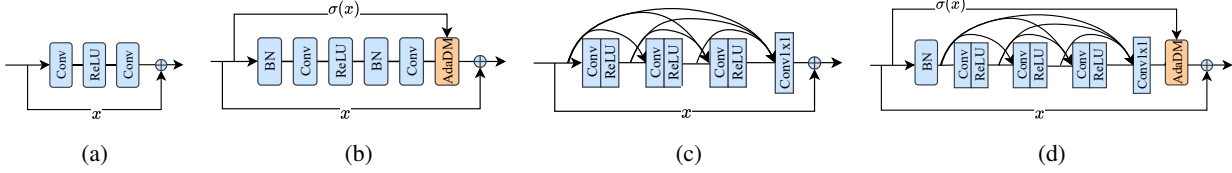


Figure 4: (a) residual block in EDSR [24] and NLSN [33]. (b) residual block with AdaDM. (c) residual dense block in RDN [49]. (d) residual dense block with AdaDM.

variation since it reflects some edge information in features. Here we compute the standard deviation (std) of γ :

$$std(\gamma) = std\left(\frac{1}{\sigma} f_{Conv}(x) - \frac{1}{\sigma} f_{Conv}(\mu I)\right) \quad (10)$$

$$= \frac{1}{\sigma} std(f_{Conv}(x)) \quad (11)$$

$$= \frac{1}{\sigma} std(y). \quad (12)$$

As we can see, the pixel deviation is reduced to $1/\sigma$ with feature normalization. The deviation is reduced because σ is usually greater than 1 (Figure 2d-2f). To compensate for the loss of pixel deviation, we multiply the γ with σ in T3. In Figure 2c, $\hat{\gamma}$ is obtained by:

$$\hat{\gamma} = \gamma \cdot \sigma, \quad (13)$$

where σ is the standard deviation of x . This process is referred to as Deviation Amplification (DA) in our paper. As a result, $\hat{\gamma}$ can keep the original pixel deviation in the presence of LN, *i.e.*, $std(\hat{\gamma}) = \sigma std(\gamma) = std(y)$.

We give the above idealized analysis to show the motivation of DA. Now, we will train three toy SR models, *i.e.*, M1, M2 and M3, by using T1, T2 and T3 to show that the DA mechanism actually works very well in reality. We adopt the EDSR [24] network and replace the body part with 32 toy residual blocks. We use 64 feature channels for fast model training. The learning curves are depicted in Figure 3. Among the three models, M2 behaves much worse than M1, which is consistent with observations in [24]. The huge performance decline comes from the added LN layer that limits the pixel deviation of the residual branch. M3 addresses this problem by using our DA mechanism and therefore achieves the best performance. Because of DA, the Conv layer in M3 can benefit from feature normalization while its output feature can also keep a regular pixel deviation. In Figure 2d-2f, we plot the deviation histograms of T1-T3 on Urban100 dataset. The standard deviation is computed on y , γ and $\hat{\gamma}$, respectively. It can be observed that T1 and T3 have similar deviation ranges while the deviation of T2 has been severely reduced, which is consistent with our analysis.

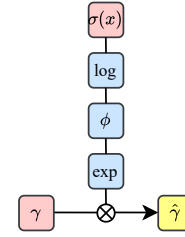


Figure 5: Schema of AdaDM.

4. Method

4.1. Adaptive Deviation Modulator

In this part, we turn to the SR models in reality. In real-world deep networks, the architecture will be much more complicated. For example, there are bias terms in each convolution and there may be non-linear layers between convolutional layers. Moreover, BN is usually applied in convolutional neural networks. It keeps separate μ and σ for each channel, which is different from LN. Though (5)-(13) may not hold for real-world cases, it gives us some insights for designing a workable solution for feature normalization. In general, we need a mechanism to recover the pixel deviation for the residual branch containing normalization layers. In order to adapt to various network architectures, we propose an Adaptive Deviation Modulator (AdaDM), enabling the network to learn the deviation amplification during training. The process of AdaDM is depicted in Figure 5 and it conducts the following computation:

$$\hat{\gamma} = \gamma \cdot e^{\phi(\log(\sigma(x)))}, \quad (14)$$

where x is the input of a residual block, and $\sigma(x)$ computes the standard deviation of x along the (C, H, W) axes (*i.e.*, one σ per 3D feature). γ is the feature needed to be modulated and $\hat{\gamma}$ is the modulated output. $\phi(v) := w \cdot v + b$ is a learnable perceptron that consists of a weight w and a bias b . During training, w and b can be updated via backpropagation algorithm. The function of ϕ is to predict a proper modulation factor according to the input scalar value v . In (14), we learn ϕ in the logarithmic space (*i.e.*, $v = \log(\sigma(x))$) for a better stability. The final modulation factor is obtained

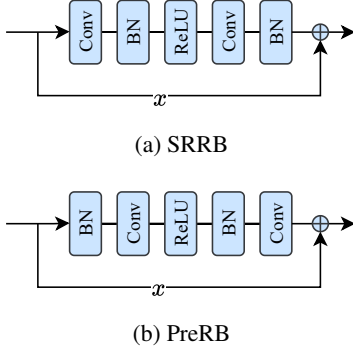


Figure 6: Two residual blocks used in Table 1 and Table 2.

by an exponential operation. In practice, w is initialized to 1 and b is initialized to 0 so that (14) can be degenerated into (13) by default. That is, the proposed AdaDM in (14) applies a more general modulation strategy than the DA in (13).

Discussion. For deviation amplification, one natural way is to compute the standard deviation and predict a modulation factor for each channel. We do not adopt this method because assigning a scaling factor to each channel involves channel interdependencies. It is difficult to distinguish whether the contribution of this method comes from channel correlation modeling or deviation amplification or both. The purpose of this paper is to verify the effectiveness of our deviation amplification mechanism, so we choose to predict a single modulation factor for the whole feature.

4.2. AdaDM with EDSR, RDN and NLSN

For fidelity image SR, it is a common practice to avoid using normalization layers in the networks. Now the network can benefit from normalization with our AdaDM. In the following, we will show how to use normalization layers and our AdaDM collaboratively in state-of-the-art networks. Due to time and computing resource constraints, we consider three SR networks, *i.e.*, EDSR [24], RDN [49] and NLSN [33]. We choose EDSR because it is widely used in image SR and its simple architecture is very suitable for method verification. RDN is selected because of the dense connections which are complicated enough to validate the effectiveness of our AdaDM. NLSN is one of the state-of-the-art SR models, which is attention-based and has excellent performance. EDSR and NLSN use the residual block in Figure 10a while RDN uses the residual dense block in Figure 4c. In Figure 10b, we add a BN layer before each convolution and insert an AdaDM layer at the end of the residual branch to build a new residual block with feature normalization, which is used in EDSR* and NLSN*. Figure 4d depicts the new residual dense block, with a BN at the front and an AdaDM at the end. This block is used in

Table 1: RB vs. SRRB

Dataset	RB	SRRB
Set5	38.22 / 0.9612	38.19 / 0.9612
Set14	33.97 / 0.9207	33.89 / 0.9200
B100	32.35 / 0.9019	32.32 / 0.9014
Urban100	32.96 / 0.9359	32.77 / 0.9343
Manga109	39.13 / 0.9778	39.00 / 0.9778

Table 2: RB vs. PreRB.

Dataset	RB	PreRB
Set5	38.22 / 0.9612	38.21 / 0.9611
Set14	33.97 / 0.9207	33.97 / 0.9209
B100	32.35 / 0.9019	32.36 / 0.9020
Urban100	32.96 / 0.9359	32.97 / 0.9360
Manga109	39.13 / 0.9778	39.17 / 0.9782

Table 3: Effects of AdaDM for $\times 2$ SR. “-/-” indicates that the model does not converge and there are no evaluation results. All the models are evaluated with PSNR / SSIM on five benchmark datasets.

Dataset	EDSR	AdaDM only	EDSR* (full)
Set5	38.22 / 0.9612	-/-	38.25 / 0.9615
Set14	33.97 / 0.9207	-/-	34.00 / 0.9205
B100	32.35 / 0.9019	-/-	32.37 / 0.9022
Urban100	32.96 / 0.9359	-/-	33.12 / 0.9371
Manga109	39.13 / 0.9778	-/-	39.31 / 0.9783

RDN*. In experiments, we will show that EDSR*, RDN* and NLSN* can achieve significant performance improvements, demonstrating the necessity of normalization for better generalization performance.

5. Experiments

5.1. Datasets and Metrics

Following [24, 49, 33], 800 training images from DIV2K [39] are used as the training dataset. All the models are evaluated on five benchmark datasets: Set5 [3], Set14 [46], B100 [31], Urban100 [13] and Manga109 [32]. The SR results are evaluated with PSNR and SSIM [44] on Y channel of transformed YCbCr space.

5.2. Training and Implementation Details

As with previous works [24, 49, 33], data augmentation is performed on the 800 training images, which are randomly rotated by 90° , 180° , 270° and flipped horizontally. In each mini-batch, 16 LR color patches with size 48×48 are cropped as the inputs. All the models are trained by ADAM [18] optimizer with $\beta_1 = 0.9$, $\beta_2 = 0.999$, and $\epsilon = 10^{-8}$. The learning rate is set to 10^{-4} and reduced to half every 200 epochs. The final model is obtained after 1000 epochs. We use the PyTorch framework to train our models with a Tesla V100 GPU. For our AdaDM, the weight w is initialized to 1 and the bias b is initialized to 0

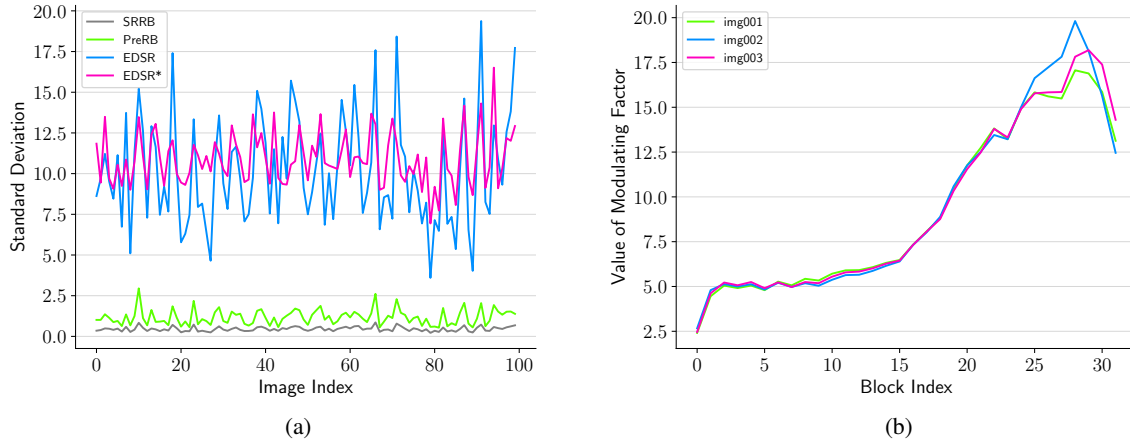


Figure 7: (a) Deviation comparisons of different models on the 100 images from Urban100 $\times 2$ dataset. The standard deviation is computed on the residual feature (*i.e.*, the feature before element-wise addition) of the last residual block. (b) Modulation factor in each residual block of EDSR* for the first three images from Urban100 $\times 2$ dataset.

as discussed in § 4.1.

5.3. Ablation Study

In this section, we conduct experiments to study the impact of individual components. For comparison, we train the EDSR model as a baseline, which is included in the second column of Table 1, Table 2 and Table 3.

Positions of BN. In [24], the authors have discussed EDSR with and without BN layers. EDSR with BN actually uses the residual block in SRResNet [20], where a BN layer is added after each convolution. We refer to the residual block in EDSR as ‘‘RB’’ (Figure 10a) and the residual block in SRResNet as ‘‘SRRB’’ (Figure 6a). Different from SRRB, we add the BN layers in front of the convolutional layers in collaboration with our AdaDM. We refer to this residual block as ‘‘PreRB’’, which is depicted in Figure 6b. It can be observed from Table 1 and Table 2 that SRRB performs much worse than RB while PreRB achieves similar results with RB. It indicates that we should place the BN layer before the convolutional layer in SR network. In PreRB, each convolution can benefit from normalized input feature and the last convolution can adjust the pixel deviation to a certain extent before adding to the identity branch. As a consequence, it performs better than SRRB. Though PreRB can keep the performance, it does not bring much improvement on benchmark datasets because of the reduced deviation. Our AdaDM can address this problem and show the usefulness of BN to improve SR performance.

Effects of AdaDM. We investigate the effects of AdaDM by removing all BN layers in EDSR*, *i.e.*, ‘‘AdaDM only’’ in Table 3. In experiments, we found that AdaDM only does

not converge at all because of huge loss values. Therefore, our AdaDM cannot work alone as a residual scaling strategy. On the contrary, it can work collaboratively with normalization layers, which demonstrates that the contribution of our AdaDM comes from deviation amplification rather than residual scaling. The last column of Table 3 shows the results of our full model. It outperforms the baseline EDSR model by a large margin on Urban100 (**+0.16dB**) and Manga109 (**+0.18dB**) datasets, which further proves the effectiveness of our AdaDM.

5.4. Analysis of Deviation Amplification

In this part, we give more analysis of the deviation amplification mechanism in AdaDM. Figure 7a depicts the deviation distributions for the models in ablation study. By comparing the four curves, we can conclude two factors that affect the performance of SR networks:

Amplitude of deviation. As shown in the bottom of Figure 7a, PreRB has more amplitude changes than SRRB. Besides, we have also known from Table 1 and Table 2 that PreRB has much better performance than SRRB. Based on these two observations, we can infer that the deviation amplitude plays a critical role in achieving good SR performance. Similar observations can also be obtained by comparing EDSR* and PreRB. EDSR* enhances the amplitude of PreRB via the proposed AdaDM.

Steadiness of deviation. EDSR* has much better performance than EDSR while its amplitude changes are smaller than the latter, which seems to violate the first conclusion. Here, we think that the performance improvements come from the regularization effects of normalization layers. Be-

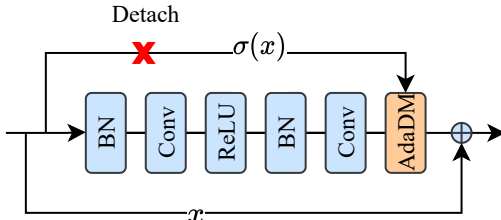


Figure 8: Detached AdaDM. The backpropagated gradients via the upper skip connection are detached.

Table 4: Quantitative comparison (average PSNR / SSIM) of AdaDM and detached AdaDM on benchmark datasets for $\times 2$ SR.

Method	Set5	Set14	B100	Urban100	Manga109
AdaDM	38.25 / 0.9615	34.00 / 0.9205	32.37 / 0.9022	33.12 / 0.9371	39.31 / 0.9783
Detached	38.26 / 0.9614	34.10 / 0.9215	32.38 / 0.9023	33.10 / 0.9371	39.26 / 0.9780

Table 5: Quantitative comparison (average PSNR / SSIM) of CRAN, DFSA and NLSN* with different training datasets for $\times 2$ SR. “†” means the results are taken from their publications.

Method	Dataset	Set5	Set14	B100	Urban100	Manga109
NLSN† [33]	DIV2K	38.34 / 0.9618	34.08 / 0.9231	32.43 / 0.9027	33.42 / 0.9394	39.59 / 0.9789
NLSN*	DIV2K	38.39 / 0.9619	34.21 / 0.9236	32.46 / 0.9031	33.59 / 0.9410	39.67 / 0.9791
CRAN† [50]	DF2K	38.31 / 0.9617	34.22 / 0.9232	32.44 / 0.9029	33.43 / 0.9394	39.75 / 0.9793
DFSA† [30]	DF2K	38.38 / 0.9620	34.33 / 0.9232	32.50 / 0.9036	33.66 / 0.9412	39.98 / 0.9798
NLSN*	DF2K	38.43 / 0.9622	34.40 / 0.9249	32.50 / 0.9036	33.78 / 0.9419	39.89 / 0.9798

Table 6: Complexity comparisons of EDSR and EDSR* on Urban100 dataset for $\times 2$ SR. Test time is estimated with the “torch.cuda.Event()” function and GPU memory is estimated with the “torch.cuda.max_memory_allocated()” function.

Method	Params	Mult-Adds	Test Time	Test Memory	Training Memory	PSNR
EDSR	40.73M	2.35T	0.72s/img	3342.74M	3813.74M	32.96dB
EDSR*	40.76M	2.35T	0.75s/img	3343.07M	7437.57M	33.12dB

cause of BN, EDSR* has a more steady deviation distribution across different images, which shows the necessity of using normalization in SR networks. This observation can also be used to explain why PreRB has a similar performance with EDSR in Table 2. Though PreRB has smaller deviation amplitudes, it has more steady deviation changes across test images. In other words, SR networks with normalization layers can have better generalization ability.

In Figure 7b, we further visualize the modulation factors in each residual block of EDSR*. For different images, the network tries to conduct similar deviation amplification at the beginning and finally predicts totally different factors for each test image, which indicates that EDSR* first exploits common feature representations and then learns specific features for HR image reconstruction.

5.5. Impact of Skip Connection

As shown in Figure 10b, we add a skip connection to compute the standard deviation of input feature. The standard deviation is used in our AdaDM for modulation factor regression. Though our AdaDM achieves substantial improvements, it is unclear whether the improvements come from deviation amplification or the added skip connection that affects the gradient backpropagation. The upper skip connection and the computation of standard deviation will bring extra gradients to the input. To eliminate this concern, we train a comparison EDSR model that uses the detached AdaDM in Figure 8. We detach the gradients of the upper skip connection during backpropagation. The comparison results are included in Table 4. We can observe that the two models perform similarly on Set5, B100 and Urban100 datasets. The detached AdaDM is 0.1dB higher on Set14 dataset and is 0.05dB lower on Manga109 dataset, which means that the detached AdaDM even has slightly better performance. Based on these observations, we can conclude that the main contribution comes from our deviation amplification during forward propagation.

5.6. Comparisons with State-of-the-Arts

The comparisons with state-of-the-art image SR models are shown in Table 7. In Table 7, EDSR*, RDN* and NLSN* denote the model using BN layers and our AdaDM in their building blocks, *i.e.*, the blocks depicted in Figure 10b and Figure 4d. For EDSR, RDN and NLSN, we include both the results from their publications (mark with “†”) and the results reproduced by us. As we can see, EDSR*, RDN* and NLSN* have much higher PSNR than their counterparts. For example, NLSN* achieves 0.3dB improvements on Manga109 dataset for $\times 4$ SR. We also show the visual comparisons of NLSN and NLSN* in Figure 9. The NLSN* can reconstruct more edge details than original NLSN.

5.7. About the Training Dataset

In this paper, we only use 800 training images from DIV2K as the training dataset and no extra training dataset is used. To show this, we train the NLSN* model with “DIV2K+Flickr2K” (DF2K) dataset for $\times 2$ SR. The evaluation results are shown in Table 5. NLSN* trained on DIV2K and Flickr2K [24] datasets shows much better performance than the model trained on DIV2K dataset. Moreover, NLSN* has much better performance than CRAN [50] and outperforms DFSA [30] on most cases.

6. Complexity Analysis

Table 6 shows the complexity comparisons of EDSR and EDSR*. As we can see, EDSR and EDSR* have similar test time and test memory consumption. The main limitation

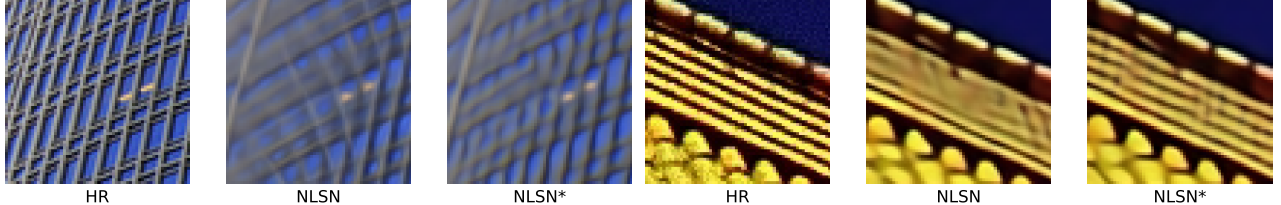


Figure 9: Visual comparisons of NLSN and NLSN* on Urban100 dataset for $\times 4$ SR.

Table 7: Quantitative comparison (average PSNR / SSIM) with state-of-the-art methods on benchmark datasets. “ \dagger ” means the results are taken from their publications, otherwise the results are from models retrained under the same experimental settings.

Method	Scale	Training Dataset	Set5		Set14		BSD100		Urban100		Manga109	
			PSNR/SSIM	PSNR/SSIM	PSNR/SSIM	PSNR/SSIM	PSNR/SSIM	PSNR/SSIM	PSNR/SSIM	PSNR/SSIM	PSNR/SSIM	PSNR/SSIM
RCAN \dagger [48]	$\times 2$	DIV2K	38.27 / 0.9614	34.12 / 0.9216	32.41 / 0.9027	33.34 / 0.9384	39.44 / 0.9786					
SAN \dagger [5]	$\times 2$	DIV2K	38.31 / 0.9620	34.07 / 0.9213	32.42 / 0.9028	33.10 / 0.9370	39.32 / 0.9792					
RFANet \dagger [27]	$\times 2$	DIV2K	38.26 / 0.9615	34.16 / 0.9220	32.41 / 0.9026	33.33 / 0.9389	39.44 / 0.9783					
HAN \dagger [35]	$\times 2$	DIV2K	38.27 / 0.9614	34.16 / 0.9217	32.41 / 0.9027	33.35 / 0.9385	39.46 / 0.9785					
IGNN \dagger [51]	$\times 2$	DIV2K	38.24 / 0.9613	34.07 / 0.9217	32.41 / 0.9025	33.23 / 0.9383	39.35 / 0.9786					
EDSR \dagger [24]	$\times 2$	DIV2K	38.11 / 0.9602	33.92 / 0.9195	32.32 / 0.9013	32.93 / 0.9351	39.10 / 0.9773					
RDN \dagger [49]	$\times 2$	DIV2K	38.24 / 0.9614	34.01 / 0.9212	32.34 / 0.9017	32.89 / 0.9353	39.18 / 0.9780					
NLSN \dagger [33]	$\times 2$	DIV2K	38.34 / 0.9618	34.08 / 0.9231	32.43 / 0.9027	33.42 / 0.9394	39.59 / 0.9789					
EDSR	$\times 2$	DIV2K	38.22 / 0.9612	33.97 / 0.9207	32.35 / 0.9019	32.96 / 0.9359	39.13 / 0.9778					
EDSR*	$\times 2$	DIV2K	38.25 / 0.9615	34.00 / 0.9205	32.37 / 0.9022	33.12 / 0.9371	39.31 / 0.9783					
RDN	$\times 2$	DIV2K	38.22 / 0.9613	33.93 / 0.9207	32.34 / 0.9017	32.89 / 0.9352	39.13 / 0.9780					
RDN*	$\times 2$	DIV2K	38.22 / 0.9612	33.99 / 0.9214	32.36 / 0.9019	33.03 / 0.9365	39.18 / 0.9778					
NLSN	$\times 2$	DIV2K	38.33 / 0.9618	34.21 / 0.9228	32.43 / 0.9028	33.45 / 0.9396	39.53 / 0.9787					
NLSN*	$\times 2$	DIV2K	38.39 / 0.9619	34.21 / 0.9236	32.46 / 0.9031	33.59 / 0.9410	39.67 / 0.9791					
RCAN \dagger [48]	$\times 3$	DIV2K	34.74 / 0.9299	30.65 / 0.8482	29.32 / 0.8111	29.09 / 0.8702	34.44 / 0.9499					
SAN \dagger [5]	$\times 3$	DIV2K	34.75 / 0.9300	30.59 / 0.8476	29.33 / 0.8112	28.93 / 0.8671	34.30 / 0.9494					
RFANet \dagger [27]	$\times 3$	DIV2K	34.79 / 0.9300	30.67 / 0.8487	29.34 / 0.8115	29.15 / 0.8720	34.59 / 0.9506					
HAN \dagger [35]	$\times 3$	DIV2K	34.75 / 0.9299	30.67 / 0.8483	29.32 / 0.8110	29.10 / 0.8705	34.48 / 0.9500					
IGNN \dagger [51]	$\times 3$	DIV2K	34.72 / 0.9298	30.66 / 0.8484	29.31 / 0.8105	29.03 / 0.8696	34.39 / 0.9496					
EDSR \dagger [24]	$\times 3$	DIV2K	34.65 / 0.9280	30.52 / 0.8462	29.25 / 0.8093	28.80 / 0.8653	34.17 / 0.9476					
RDN \dagger [49]	$\times 3$	DIV2K	34.71 / 0.9296	30.57 / 0.8468	29.26 / 0.8093	28.80 / 0.8653	34.13 / 0.9484					
NLSN \dagger [33]	$\times 3$	DIV2K	34.85 / 0.9306	30.70 / 0.8485	29.34 / 0.8117	29.25 / 0.8726	34.57 / 0.9508					
EDSR	$\times 3$	DIV2K	34.70 / 0.9295	30.56 / 0.8465	29.26 / 0.8097	28.85 / 0.8663	34.05 / 0.9483					
EDSR*	$\times 3$	DIV2K	34.81 / 0.9302	30.63 / 0.8481	29.31 / 0.8108	29.02 / 0.8693	34.48 / 0.9499					
RDN	$\times 3$	DIV2K	34.70 / 0.9295	30.56 / 0.8464	29.26 / 0.8092	28.80 / 0.8654	34.11 / 0.9483					
RDN*	$\times 3$	DIV2K	34.79 / 0.9300	30.62 / 0.8477	29.28 / 0.8097	28.95 / 0.8676	34.29 / 0.9490					
NLSN	$\times 3$	DIV2K	34.90 / 0.9310	30.74 / 0.8495	29.37 / 0.8126	29.34 / 0.8746	34.64 / 0.9513					
NLSN*	$\times 3$	DIV2K	34.94 / 0.9313	30.80 / 0.8503	29.40 / 0.8130	29.53 / 0.8775	34.95 / 0.9524					
RCAN \dagger [48]	$\times 4$	DIV2K	32.63 / 0.9002	28.87 / 0.7889	27.77 / 0.7436	26.82 / 0.8087	31.22 / 0.9173					
SAN \dagger [5]	$\times 4$	DIV2K	32.64 / 0.9003	28.92 / 0.7888	27.78 / 0.7436	26.79 / 0.8068	31.18 / 0.9169					
RFANet \dagger [27]	$\times 4$	DIV2K	32.66 / 0.9004	28.88 / 0.7894	27.79 / 0.7442	26.92 / 0.8112	31.41 / 0.9187					
HAN \dagger [35]	$\times 4$	DIV2K	32.64 / 0.9002	28.90 / 0.7890	27.80 / 0.7442	26.85 / 0.8094	31.42 / 0.9177					
IGNN \dagger [51]	$\times 4$	DIV2K	32.57 / 0.8998	28.85 / 0.7891	27.77 / 0.7434	26.84 / 0.8090	31.28 / 0.9182					
EDSR \dagger [24]	$\times 4$	DIV2K	32.46 / 0.8968	28.80 / 0.7876	27.71 / 0.7420	26.64 / 0.8033	31.02 / 0.9148					
RDN \dagger [49]	$\times 4$	DIV2K	32.47 / 0.8990	28.81 / 0.7871	27.72 / 0.7419	26.61 / 0.8028	31.00 / 0.9151					
NLSN \dagger [33]	$\times 4$	DIV2K	32.59 / 0.9000	28.87 / 0.7891	27.78 / 0.7444	26.96 / 0.8109	31.27 / 0.9184					
EDSR	$\times 4$	DIV2K	32.51 / 0.8985	28.78 / 0.7872	27.73 / 0.7419	26.66 / 0.8040	31.04 / 0.9152					
EDSR*	$\times 4$	DIV2K	32.59 / 0.8995	28.87 / 0.7887	27.76 / 0.7433	26.83 / 0.8079	31.24 / 0.9172					
RDN	$\times 4$	DIV2K	32.48 / 0.8988	28.81 / 0.7869	27.72 / 0.7411	26.62 / 0.8023	31.03 / 0.9154					
RDN*	$\times 4$	DIV2K	32.49 / 0.8991	28.84 / 0.7883	27.74 / 0.7423	26.72 / 0.8056	31.18 / 0.9171					
NLSN	$\times 4$	DIV2K	32.65 / 0.9009	28.93 / 0.7900	27.82 / 0.7453	27.06 / 0.8147	31.43 / 0.9202					
NLSN*	$\times 4$	DIV2K	32.75 / 0.9018	28.96 / 0.7917	27.85 / 0.7464	27.24 / 0.8182	31.73 / 0.9225					

is the training memory required by EDSR*. If the training time memory consumption is not a problem, the proposed normalization technique can bring a significant performance improvement while not affecting the test time and memory much.

7. Conclusion

In this paper, we give a comprehensive analysis of feature normalization in image Super-Resolution (SR) networks. We found that the performance degradation caused by normalization layers comes from the reduced pixel deviation of residual features. When the pixel deviation shrinks, the variation of pixel values becomes smaller, making the edges less discriminative for the network to resolve. To address this problem, we propose an Adaptive Deviation Modulator (AdaDM) that can amplify the pixel deviation of normalized residual features. Thanks to our AdaDM, we successfully apply normalization layers to state-of-the-art SR networks and achieve substantial performance improvements.

A1. About the RGB Range

As we have analyzed in the paper that normalization layers in SR networks will reduce the pixel deviation by dividing by a σ . In practice, we can adopt the RGB range of 255 (*i.e.*, $[0, 255]$) or 1 (*i.e.*, $[0, 1]$) for model training. When we choose the training RGB range of 1, pixel scaling occurs implicitly. In the following, we will investigate whether the training RGB range has an impact on performance. Figure 10a shows the training curves of EDSR+BN with RGB range of 255 and 1, respectively. When training with RGB range of 1, EDSR+BN becomes unstable and it converges much worse than training with RGB range of 255. Therefore, it is better to use RGB range of 255 when training with BN in SR networks since BN will further reduce the pixel deviation. Figure 10b shows the training curves of original EDSR and EDSR*. Different from EDSR+BN, the training RGB range has little impact on original EDSR model since it removes the BN layers in residual blocks. Our EDSR* has almost the same performance when training with different RGB ranges, which indicates that our AdaDM is effective enough in deviation amplification and it is robust to training RGB ranges.

A2. Results for DF2K Dataset

In Table 8, Table 9 and Table 10, we include the evaluation results of NLSN* trained on DIV2K+Fllickr2K (DF2K) dataset for $\times 2$, $\times 3$ and $\times 4$ SR, respectively. As we can see, the performance of NLSN* can be further improved when trained on DF2K dataset, which shows that the proposed normalization strategy can also work with large training dataset with variety of texture details.

Table 8: Quantitative comparison (average PSNR / SSIM) of NLSN [33] and SwinIR [23] with different training datasets for $\times 2$ SR. “+” means the results are obtained with self-ensemble testing.

Method	Dataset	Set5	Set14	B100	Urban100	Manga109
NLSN*	DIV2K	38.39 / 0.9619	34.21 / 0.9236	32.46 / 0.9031	33.59 / 0.9410	39.67 / 0.9791
NLSN*+	DIV2K	38.43 / 0.9621	34.37 / 0.9245	32.50 / 0.9036	33.83 / 0.9424	39.83 / 0.9795
SwinIR+	DF2K	38.46 / 0.9624	34.61 / 0.9260	32.55 / 0.9043	33.95 / 0.9433	40.02 / 0.9800
NLSN*	DF2K	38.43 7 / 0.9622	34.40 / 0.9249	32.50 / 0.9036	33.78 / 0.9419	39.89 / 0.9798
NLSN*+	DF2K	38.50 / 0.9624	34.46 / 0.9255	32.53 / 0.9040	33.96 / 0.9431	40.03 / 0.9801

Table 9: Quantitative comparison (average PSNR / SSIM) of NLSN [33] and SwinIR [23] with different training datasets for $\times 3$ SR. “+” means the results are obtained with self-ensemble testing.

Method	Dataset	Set5	Set14	B100	Urban100	Manga109
NLSN*	DIV2K	34.94 / 0.9131	30.80 / 0.8503	29.40 / 0.8130	29.53 / 0.8775	34.95 / 0.9524
NLSN*+	DIV2K	35.00 / 0.9138	30.89 / 0.8519	29.45 / 0.8139	29.74 / 0.8803	35.19 / 0.9535
SwinIR+	DF2K	35.04 / 0.9322	31.00 / 0.8542	29.49 / 0.8150	29.90 / 0.8841	35.28 / 0.9543
NLSN*+	DF2K	34.95 7 / 0.9316	30.86 / 0.8513	29.45 / 0.8141	29.77 / 0.8812	35.20 / 0.9534
NLSN*+	DF2K	35.04 / 0.9320	30.96 / 0.8528	29.49 / 0.8148	29.94 / 0.8832	35.40 / 0.9542

Table 10: Quantitative comparison (average PSNR / SSIM) of NLSN [33] and SwinIR [23] with different training datasets for $\times 4$ SR. “+” means the results are obtained with self-ensemble testing.

Method	Dataset	Set5	Set14	B100	Urban100	Manga109
NLSN*	DIV2K	32.75 / 0.9018	28.96 / 0.7917	27.85 / 0.7464	27.24 / 0.8182	31.73 / 0.9225
NLSN*+	DIV2K	32.94 / 0.9036	29.10 / 0.7936	27.92 / 0.7482	27.47 / 0.8230	32.10 / 0.9253
SwinIR+	DF2K	32.93 7 / 0.9043	29.15 / 0.7958	27.95 / 0.7494	27.56 / 0.8273	32.22 / 0.9273
NLSN*+	DF2K	32.86 7 / 0.9025	29.11 7 / 0.7940	27.92 7 / 0.7481	27.49 7 / 0.8247	32.09 / 0.9251
NLSN*+	DF2K	32.99 / 0.9037	29.19 / 0.7952	27.97 / 0.7490	27.66 / 0.8279	32.34 / 0.9269

A3. Self-Ensemble Results

It is well known that the performance of SR network could be greatly improved with self-ensemble strategy. To show this, we also include the self-ensemble results of NLSN* in Table 8, Table 9 and Table 10 for $\times 2$, $\times 3$ and $\times 4$ SR, respectively. The models with self-ensemble strategy are marked by “+”. Both NLSN* models trained on DIV2K dataset and DF2K dataset can get substantial performance improvements with self-ensemble testing strategy.

A4. Comparison with SwinIR

Recently, Transformer-based [41] models become the leading methods for various of computer vision tasks. In image SR, the Swin Transformer [29] based SwinIR [23] network achieved significant performance improvements compared with traditional CNN-based models. We also compare the NLSN* with SwinIR in Table 8, Table 9 and Table 10. Both NLSN*+ and SwinIR+ are trained on DF2K dataset. It can be observed that NLSN*+ can achieve comparable results with SwinIR+ on benchmark datasets, which shows the effectiveness of our AdaDM in boosting the SR performance. With our AdaDM, the CNN-based NLSN [33] network can even match the performance of Transformer-based SwinIR network.

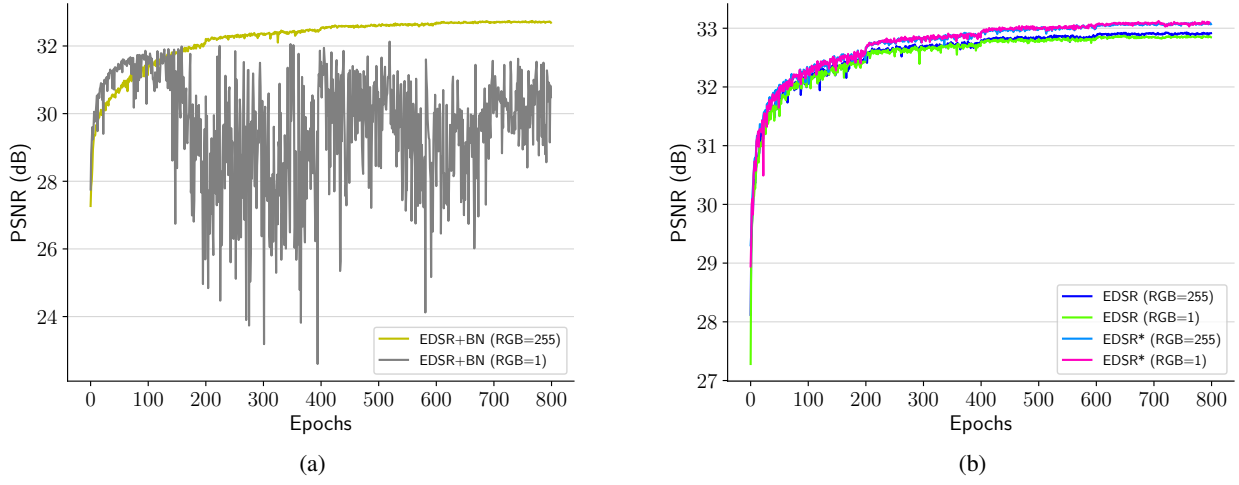


Figure 10: Training curves of EDSR, EDSR+BN and EDSR*.

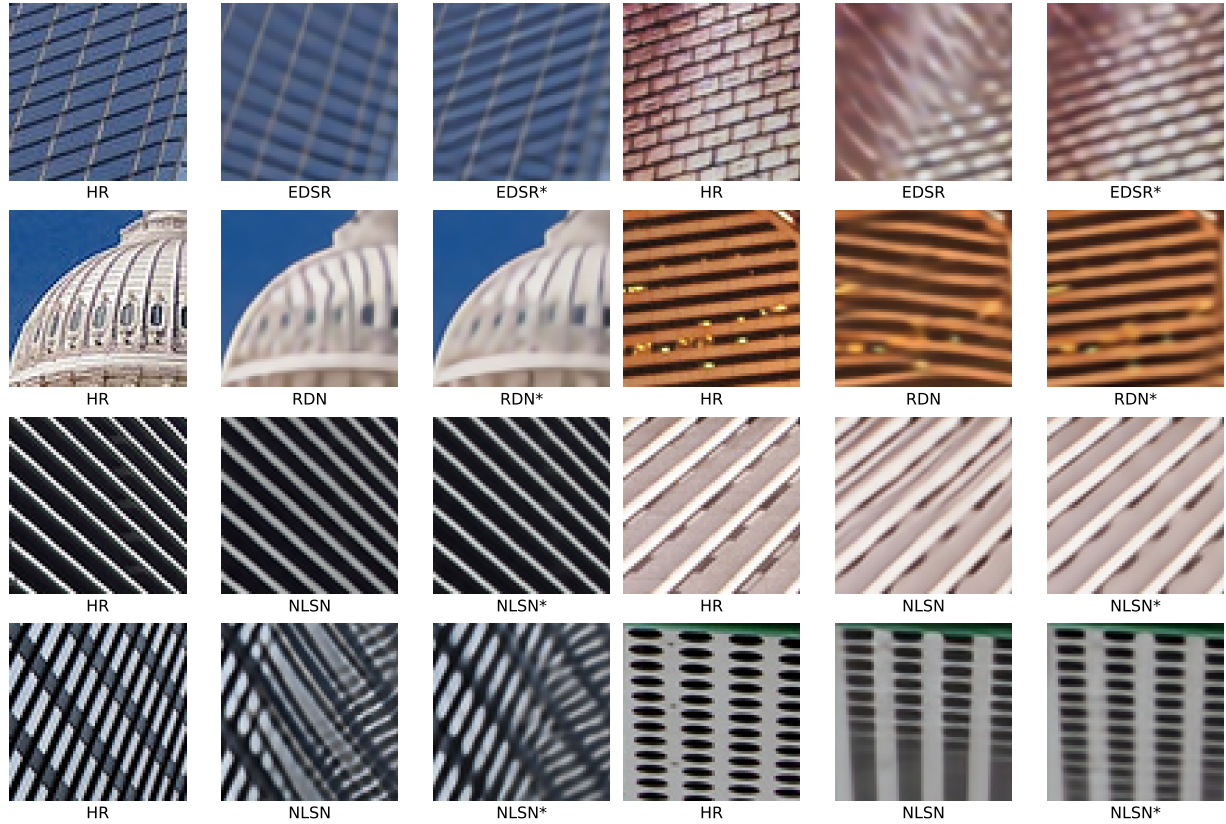


Figure 11: More visual results on Urban100 $\times 4$ dataset

A5. More Visual Results

Our AdaDM can reconstruct the edges in images very well. To verify this, we show more visual comparison re-

sults in Figure 11. As we can see, the models with our AdaDM can recover the edges much better than original models.

References

[1] Namhyuk Ahn, Byungkon Kang, and Kyung-Ah Sohn. Fast, accurate, and lightweight super-resolution with cascading residual network. In *ECCV (10)*, volume 11214 of *Lecture Notes in Computer Science*, pages 256–272. Springer, 2018. [1](#)

[2] Lei Jimmy Ba, Jamie Ryan Kiros, and Geoffrey E. Hinton. Layer normalization. *arXiv preprint*, arXiv:1607.06450, 2016. [2](#)

[3] Marco Bevilacqua, Aline Roumy, Christine Guillemot, and Marie-Line Alberi-Morel. Low-complexity single-image super-resolution based on nonnegative neighbor embedding. In *BMVC*, pages 1–10. BMVA Press, 2012. [5](#)

[4] Hanting Chen, Yunhe Wang, Tianyu Guo, Chang Xu, Yiping Deng, Zhenhua Liu, Siwei Ma, Chunjing Xu, Chao Xu, and Wen Gao. Pre-trained image processing transformer. In *CVPR*, pages 12299–12310. Computer Vision Foundation / IEEE, 2021. [2](#)

[5] Tao Dai, Jianrui Cai, Yongbing Zhang, Shu-Tao Xia, and Lei Zhang. Second-order attention network for single image super-resolution. In *CVPR*, pages 11065–11074. Computer Vision Foundation / IEEE, 2019. [2, 8](#)

[6] Chao Dong, Chen Change Loy, Kaiming He, and Xiaoou Tang. Learning a deep convolutional network for image super-resolution. In *ECCV (4)*, volume 8692 of *Lecture Notes in Computer Science*, pages 184–199. Springer, 2014. [1, 2](#)

[7] Chao Dong, Chen Change Loy, and Xiaoou Tang. Accelerating the super-resolution convolutional neural network. In *ECCV (2)*, volume 9906 of *Lecture Notes in Computer Science*, pages 391–407. Springer, 2016. [1, 2](#)

[8] Yong Guo, Jian Chen, Jingdong Wang, Qi Chen, Jiezhang Cao, Zeshuai Deng, Yanwu Xu, and Mingkui Tan. Closed-loop matters: Dual regression networks for single image super-resolution. In *CVPR*, pages 5406–5415. Computer Vision Foundation / IEEE, 2020. [1](#)

[9] Muhammad Haris, Gregory Shakhnarovich, and Norimichi Ukita. Deep back-projection networks for super-resolution. In *CVPR*, pages 1664–1673. IEEE Computer Society, 2018. [2](#)

[10] Kaiming He, Xiangyu Zhang, Shaoqing Ren, and Jian Sun. Deep residual learning for image recognition. In *CVPR*, pages 770–778. IEEE Computer Society, 2016. [1, 2](#)

[11] Xiangyu He, Zitao Mo, Peisong Wang, Yang Liu, Mingyuan Yang, and Jian Cheng. Ode-inspired network design for single image super-resolution. In *CVPR*, pages 1732–1741. Computer Vision Foundation / IEEE, 2019. [2](#)

[12] Gao Huang, Zhuang Liu, Laurens van der Maaten, and Kilian Q. Weinberger. Densely connected convolutional networks. In *CVPR*, pages 2261–2269. IEEE Computer Society, 2017. [2](#)

[13] Jia-Bin Huang, Abhishek Singh, and Narendra Ahuja. Single image super-resolution from transformed self-exemplars. In *CVPR*, pages 5197–5206. IEEE Computer Society, 2015. [5](#)

[14] Zheng Hui, Xinbo Gao, Yunchu Yang, and Xiumei Wang. Lightweight image super-resolution with information multi-distillation network. In *ACM Multimedia*, pages 2024–2032. ACM, 2019. [1](#)

[15] Sergey Ioffe and Christian Szegedy. Batch normalization: Accelerating deep network training by reducing internal covariate shift. In *ICML*, volume 37 of *JMLR Workshop and Conference Proceedings*, pages 448–456. JMLR.org, 2015. [2](#)

[16] Jiwon Kim, Jung Kwon Lee, and Kyoung Mu Lee. Accurate image super-resolution using very deep convolutional networks. In *CVPR*, pages 1646–1654. IEEE Computer Society, 2016. [2](#)

[17] Jiwon Kim, Jung Kwon Lee, and Kyoung Mu Lee. Deeply-recursive convolutional network for image super-resolution. In *CVPR*, pages 1637–1645. IEEE Computer Society, 2016. [2](#)

[18] Diederik P. Kingma and Jimmy Ba. Adam: A method for stochastic optimization. *arXiv preprint*, arXiv:1412.6980, 2014. [5](#)

[19] Wei-Sheng Lai, Jia-Bin Huang, Narendra Ahuja, and Ming-Hsuan Yang. Deep laplacian pyramid networks for fast and accurate super-resolution. In *CVPR*, pages 5835–5843. IEEE Computer Society, 2017. [2](#)

[20] Christian Ledig, Lucas Theis, Ferenc Huszar, Jose Caballero, Andrew Cunningham, Alejandro Acosta, Andrew P. Aitken, Alykhan Tejani, Johannes Totz, Zehan Wang, and Wenzhe Shi. Photo-realistic single image super-resolution using a generative adversarial network. In *CVPR*, pages 105–114. IEEE Computer Society, 2017. [1, 2, 6](#)

[21] Wonkyung Lee, Junghyup Lee, Dohyung Kim, and Bumsub Ham. Learning with privileged information for efficient image super-resolution. In *ECCV (24)*, volume 12369 of *Lecture Notes in Computer Science*, pages 465–482. Springer, 2020. [1](#)

[22] Zhen Li, Jinglei Yang, Zheng Liu, Xiaomin Yang, Gwanggil Jeon, and Wei Wu. Feedback network for image super-resolution. In *CVPR*, pages 3867–3876. Computer Vision Foundation / IEEE, 2019. [2](#)

[23] Jingyun Liang, Jiezhang Cao, Guolei Sun, Kai Zhang, Luc Van Gool, and Radu Timofte. Swinir: Image restoration using swin transformer. *arXiv preprint*, arXiv:2108.10257, 2021. [2, 9](#)

[24] Bee Lim, Sanghyun Son, Heewon Kim, Seungjun Nah, and Kyoung Mu Lee. Enhanced deep residual networks for single image super-resolution. In *CVPR Workshops*, pages 1132–1140. IEEE Computer Society, 2017. [1, 2, 4, 5, 6, 7, 8](#)

[25] Ding Liu, Bihan Wen, Yuchen Fan, Chen Change Loy, and Thomas S. Huang. Non-local recurrent network for image restoration. In *NeurIPS*, pages 1680–1689, 2018. [2](#)

[26] Jie Liu, Jie Tang, and Gangshan Wu. Residual feature distillation network for lightweight image super-resolution. In *ECCV Workshops (3)*, volume 12537 of *Lecture Notes in Computer Science*, pages 41–55. Springer, 2020. [2](#)

[27] Jie Liu, Wenjie Zhang, Yuting Tang, Jie Tang, and Gangshan Wu. Residual feature aggregation network for image super-resolution. In *CVPR*, pages 2356–2365. Computer Vision Foundation / IEEE, 2020. [2, 8](#)

[28] Jie Liu, Minqiang Zou, Jie Tang, and Gangshan Wu. Memory recursive network for single image super-resolution. In *ACM Multimedia*, pages 2202–2210. ACM, 2020. [2](#)

[29] Ze Liu, Yutong Lin, Yue Cao, Han Hu, Yixuan Wei, Zheng Zhang, Stephen Lin, and Baining Guo. Swin transformer: Hierarchical vision transformer using shifted windows. In *Proceedings of the IEEE/CVF International Conference on Computer Vision (ICCV)*, pages 10012–10022, October 2021. [9](#)

[30] Salma Abdel Magid, Yulun Zhang, Donglai Wei, Won-Dong Jang, Zudi Lin, Yun Fu, and Hanspeter Pfister. Dynamic high-pass filtering and multi-spectral attention for image super-resolution. In *Proceedings of the IEEE/CVF International Conference on Computer Vision (ICCV)*, pages 4288–4297, October 2021. [2, 7](#)

[31] David R. Martin, Charless C. Fowlkes, Doron Tal, and Jitendra Malik. A database of human segmented natural images and its application to evaluating segmentation algorithms and measuring ecological statistics. In *ICCV*, pages 416–425, 2001. [5](#)

[32] Yusuke Matsui, Kota Ito, Yuji Aramaki, Azuma Fujimoto, Toru Ogawa, Toshihiko Yamasaki, and Kiyoharu Aizawa. Sketch-based manga retrieval using manga109 dataset. *Multimedia Tools Appl.*, 76(20):21811–21838, 2017. [5](#)

[33] Yiqun Mei, Yuchen Fan, and Yuqian Zhou. Image super-resolution with non-local sparse attention. In *CVPR*, pages 3517–3526. Computer Vision Foundation / IEEE, 2021. [1, 2, 4, 5, 7, 8, 9](#)

[34] Yiqun Mei, Yuchen Fan, Yuqian Zhou, Lichao Huang, Thomas S. Huang, and Honghui Shi. Image super-resolution with cross-scale non-local attention and exhaustive self-exemplars mining. In *CVPR*, pages 5689–5698. Computer Vision Foundation / IEEE, 2020. [2](#)

[35] Ben Niu, Weilei Wen, Wenqi Ren, Xiangde Zhang, Lianping Yang, Shuzhen Wang, Kaihao Zhang, Xiaochun Cao, and Haifeng Shen. Single image super-resolution via a holistic attention network. In *ECCV (12)*, volume 12357 of *Lecture Notes in Computer Science*, pages 191–207. Springer, 2020. [2, 8](#)

[36] Wenzhe Shi, Jose Caballero, Ferenc Huszar, Johannes Totz, Andrew P. Aitken, Rob Bishop, Daniel Rueckert, and Zehan Wang. Real-time single image and video super-resolution using an efficient sub-pixel convolutional neural network. In *CVPR*, pages 1874–1883. IEEE Computer Society, 2016. [2](#)

[37] Dehua Song, Yunhe Wang, Hanting Chen, Chang Xu, Chunjing Xu, and Dacheng Tao. Adders: Towards energy efficient image super-resolution. In *CVPR*, pages 15648–15657. Computer Vision Foundation / IEEE, 2021. [2](#)

[38] Ying Tai, Jian Yang, Xiaoming Liu, and Chunyan Xu. Memnet: A persistent memory network for image restoration. In *ICCV*, pages 4549–4557. IEEE Computer Society, 2017. [2](#)

[39] Radu Timofte, Eirikur Agustsson, Luc Van Gool, Ming-Hsuan Yang, Lei Zhang, Bee Lim, Sanghyun Son, Heewon Kim, Seungjun Nah, Kyoung Mu Lee, et al. NTIRE 2017 challenge on single image super-resolution: Methods and results. In *CVPR Workshops*, pages 1110–1121. IEEE Computer Society, 2017. [5](#)

[40] Dmitry Ulyanov, Andrea Vedaldi, and Victor S. Lempitsky. Instance normalization: The missing ingredient for fast stylization. *CoRR*, abs/1607.08022, 2016. [2](#)

[41] Ashish Vaswani, Noam Shazeer, Niki Parmar, Jakob Uszkoreit, Llion Jones, Aidan N. Gomez, Łukasz Kaiser, and Illia Polosukhin. Attention is all you need. In *NIPS*, pages 5998–6008, 2017. [9](#)

[42] Longguang Wang, Yingqian Wang, Zaiping Lin, Jungang Yang, Wei An, and Yulan Guo. Learning a single network for scale-arbitrary super-resolution. In *Proceedings of the IEEE/CVF International Conference on Computer Vision (ICCV)*, pages 4801–4810, October 2021. [1](#)

[43] Xintao Wang, Ke Yu, Shixiang Wu, Jinjin Gu, Yihao Liu, Chao Dong, Yu Qiao, and Chen Change Loy. ESRGAN: enhanced super-resolution generative adversarial networks. In *ECCV Workshops (5)*, volume 11133 of *Lecture Notes in Computer Science*, pages 63–79. Springer, 2018. [2](#)

[44] Zhou Wang, Alan C. Bovik, Hamid R. Sheikh, and Eero P. Simoncelli. Image quality assessment: from error visibility to structural similarity. *IEEE Trans. Image Processing*, 13(4):600–612, 2004. [5](#)

[45] Yuxin Wu and Kaiming He. Group normalization. In *ECCV (13)*, volume 11217 of *Lecture Notes in Computer Science*, pages 3–19. Springer, 2018. [2](#)

[46] Roman Zeyde, Michael Elad, and Matan Protter. On single image scale-up using sparse-representations. In *Curves and Surfaces*, volume 6920 of *Lecture Notes in Computer Science*, pages 711–730. Springer, 2010. [5](#)

[47] Kai Zhang, Wangmeng Zuo, and Lei Zhang. Learning a single convolutional super-resolution network for multiple degradations. In *CVPR*, pages 3262–3271. Computer Vision Foundation / IEEE Computer Society, 2018. [2](#)

[48] Yulun Zhang, Kunpeng Li, Kai Li, Lichen Wang, Bineng Zhong, and Yun Fu. Image super-resolution using very deep residual channel attention networks. In *ECCV (7)*, volume 11211 of *Lecture Notes in Computer Science*, pages 294–310. Springer, 2018. [2, 8](#)

[49] Yulun Zhang, Yapeng Tian, Yu Kong, Bineng Zhong, and Yun Fu. Residual dense network for image super-resolution. In *CVPR*, pages 2472–2481. Computer Vision Foundation / IEEE Computer Society, 2018. [1, 2, 4, 5, 8](#)

[50] Yulun Zhang, Donglai Wei, Can Qin, Huan Wang, Hanspeter Pfister, and Yun Fu. Context reasoning attention network for image super-resolution. In *Proceedings of the IEEE/CVF International Conference on Computer Vision (ICCV)*, pages 4278–4287, October 2021. [2, 7](#)

[51] Shangchen Zhou, Jiawei Zhang, Wangmeng Zuo, and Chen Change Loy. Cross-scale internal graph neural network for image super-resolution. In *NeurIPS*, 2020. [8](#)